

Swimming in a Crystal: Hydrodynamic, Phoretic and Steric Interactions

Aidan T. Brown,¹ Ioana D. Vladescu,¹ Angela Dawson,¹ Teun Vissers,¹
 Jana Schwarz-Linek,¹ Juho S. Lintuvuori,^{1,2} and Wilson C. K. Poon¹

¹*SUPA, School of Physics and Astronomy, The University of Edinburgh,
 King's Buildings, Peter Guthrie Tait Road, Edinburgh, EH9 3FD, United Kingdom*

²*Laboratoire de Physique des Solides, Université Paris-Sud, UMR 8502 - 91405 Orsay, France*

We study catalytic Janus swimmers and *E. coli* bacteria in a 2D colloidal crystal. The Janus swimmers orbit individual colloids and hop between colloids stochastically. Their orbital speed oscillates periodically. We show why swimming-associated phoretic gradients are unlikely to be the cause of these oscillations; instead, they are likely due to hydrodynamic interactions, and suggest that our swimmers are ‘pushers’. We find little evidence implicating hydrodynamic interactions in the stability of the orbital trapping itself. Motile *E. coli* bacteria behave very differently in the same colloidal crystal: their circular orbits on plain glass are rectified into long, straight runs, because the bacteria are unable to turn corners inside the crystal.

Understanding non-equilibrium systems is a grand challenge cutting across many areas of physics. An exciting frontier concerns microscopic swimmers, from biological swimmers such as motile bacteria and algae, to synthetic self-propelled colloids [1, 2]. There has been much recent theoretical and experimental study of the many-body physics of such swimmers [3], and for this purpose it is important to understand how these swimmers interact.

The simplest interactions are steric: two swimmers cannot overlap. Steric interactions coupled with a lack of detailed balance already generate a host of interesting phenomena, e.g. phase separation [4, 5], collective motion [6], and rectification [7, 8]. However, hydrodynamic interactions (HI) can produce qualitatively different behavior in fluids compared to steric interactions [3, 9]. Thus, e.g., HI can suppress steric-induced phase separation [10], and, depending on the swimmers’ specific flow-fields, either reduce or increase the effective fluid viscosity [9].

For understanding most biological swimmers, HI and steric interactions may be sufficient, because the biochemical machinery is typically internal. By contrast, the propulsion of synthetic colloids often also depends on self-generated external gradients, which produce further ‘phoretic interactions’ (PI) [11–13]. These must be understood to interpret collective behavior correctly in synthetic swimmers [13–16].

One can gain insight into such interactions in a variety of ways: by studying swimmer-swimmer interactions directly in dilute suspensions [17], but also by looking at the interactions between swimmers and passive tracer particles [18–20], surfaces [12, 21–25] or porous media [26, 27], which are all also of intrinsic interest.

In this Letter, we study the interactions of a popular phoretic swimmer, catalytic Pt-coated Janus particles fuelled by H_2O_2 [28], with a 2D crystal of passive colloids. This swimmer was originally proposed to swim via self-diffusiophoresis, where gradients of O_2 or H_2O_2 drive the motion [28, 29]. The subsequent observation of strong ionic effects [16, 30, 31], and the diffusiophoretic mecha-

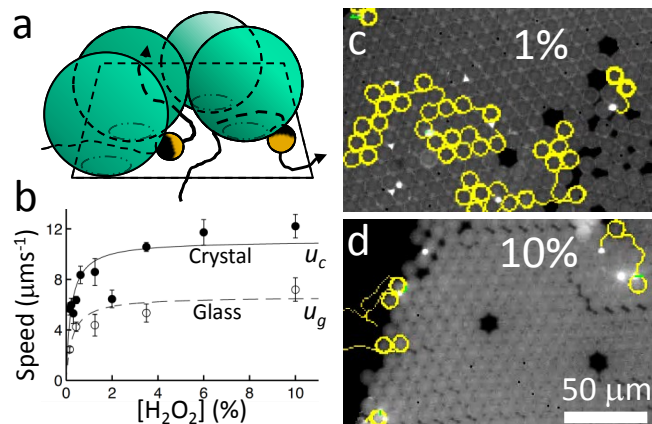


FIG. 1. a) Schematic of experimental setup. b) Mean ballistic speed u inside (u_c , \bullet), and outside (u_g , \circ) crystal. Solid and dashed lines: predicted forms if H_2O_2 decomposition is limited by catalytic site availability on Pt [28]: $u = u_{max} [H_2O_2] / ([H_2O_2]_0 + [H_2O_2])$, with u_{max} and $[H_2O_2]_0$ constants. c) Tracked video of Janus swimmers inside a colloidal crystal at 1% and d) at 10% H_2O_2 , over 3 minutes.

nism’s low theoretical efficiency [30], make this unlikely. We instead proposed a self-electrophoretic model [30] in which self-generated electric fields drive motion, as in [32].

In colloidal crystals, we find, first, that these swimmers are trapped in orbits around individual colloids, as seen for Pt-Au nano-rod swimmers [26]. While in orbit, they display periodic speed oscillations due to interactions with neighbouring colloids. Modelling the phoretic propulsion of these swimmers, we find that these oscillations are most consistent with a swimmer which is a pusher, i.e. one that pushes fluid out fore and aft along its swimming axis. Calculations show that for self-electrophoretic swimmers, PI should be insignificant compared to HI, whereas self-diffusiophoretic swimmers would experience strong PI associated with the fuel consumption rate.

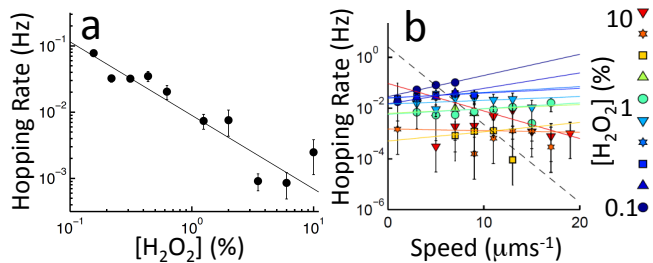


FIG. 2. a) Hopping rate vs. $[\text{H}_2\text{O}_2]$. Solid line: $\Gamma \propto [\text{H}_2\text{O}_2]^{-1}$. b) Hopping rate binned by speed for each $[\text{H}_2\text{O}_2]$ (colour-coded). Solid lines: exponential fits within each $[\text{H}_2\text{O}_2]$; dashed line: exponential fit through the mean of each dataset.

Secondly, the rate at which Janus swimmers hop between orbits around neighbouring colloids in the crystal is inversely dependent on $[\text{H}_2\text{O}_2]$. However, we find no dependence of this hopping rate on swimming speed, indicating that orbital trapping may be PI-dominated.

Finally, *E. coli* swimming in the same colloidal crystals display opposite behavior to Janus swimmers. The normal orbital motion of *E. coli* on plain glass [33–35] is rectified into straight trajectories by the crystal, which can be explained simply by steric effects.

We prepared Janus particles (5 nm Pt sputtered on 2 μm diameter fluorescent polystyrene colloids (Invitrogen) [30]) and suspended them at volume fraction $\sim 10^{-6}$ in aqueous H_2O_2 (Acros) solutions in chambers formed between glass slides (Menzel) and $22 \times 22 \text{ mm}^2$ glass coverslips (Bettering) with 300 μm thick parafilm spacers. On the coverslips, 2D colloidal crystals were formed beforehand by depositing 10 μm diameter polystyrene colloids (Thermo-Fisher) at 1% v/v in water and evaporating at 70°C. The radii of the static colloids, $R = 5.06 \pm 0.02 \mu\text{m}$, and Janus swimmers, $a = 0.96 \pm 0.04 \mu\text{m}$, were determined by repeated (25 \times) measurement of interparticle distances in close-packed 2D crystals.

These Janus swimmers are bottom-heavy, and so swim upwards [30, 36], so we initially allowed them to collect at the upper, coated coverslip, before inverting the chamber for observation in an inverted epifluorescence microscope (Ti Eclipse, Nikon, $\times 20$ objective) with a CCD camera (Eosens, Mikrotron). This inversion left swimmer behavior unchanged. They swim stably along the coverslip surface [30]. On colliding with a colloid at the edge of the crystal they orbit that colloid in the wedge-like space between colloid and coverslip, Fig. 1a, before hopping out of the crystal or into orbit around another colloid.

Tuning the swimming speed with $[\text{H}_2\text{O}_2]$ [28], Fig. 1b, permits detailed study of this orbital behavior. Note first that the speed inside the crystal, $u_c > u_g$, the speed on plain glass, with $u_c/u_g = 1.7 \pm 0.3$. Tracking (using MATLAB [30, 37]) reveals that the rate Γ , at which a swimmer hops between orbits centred on neighbouring colloids scales as $\Gamma \propto [\text{H}_2\text{O}_2]^{-1}$ (Fig. 2a). Thus, in

1% $[\text{H}_2\text{O}_2]$, swimmers hop rapidly through the crystal (Fig. 1c and supplementary video SV1 [38]), whereas in 10% H_2O_2 , they remain near the crystal’s edge for many minutes (Fig. 1d). We will return to this observation below.

In 10% H_2O_2 , orbits are stable for 100s of revolutions, and tracking (with $\times 100$ objective, see SV2 [38]), revealed sinusoidal speed oscillations u' around the mean speed u_c (Fig. 3b), of the form: $u'/u_c = \tilde{u} \cos[6(\phi - \delta)]$, with $\delta \in (-30^\circ, 30^\circ]$. The orbital angle ϕ is defined so that the 6 neighbouring colloids are at $\phi = 0^\circ, 60^\circ$, etc. We measure from 17 videos a fractional amplitude $\tilde{u} = 7.7 \pm 0.5\%$ and retardation $\delta = 13.5 \pm 1.5^\circ$.

Only a few types of long-range interactions which could account for these oscillations. To rule out direct electrostatic interactions, we added 100 μM NaNO_3 . This left the oscillations unchanged. However, the observed oscillations of $\sim 1 \mu\text{m s}^{-1}$, if electrostatic in origin, would require charge densities of $\sigma > 1 \text{ Cm}^{-2}$, far larger than normal for colloidal systems ($\sigma \sim 10^{-4} \text{ Cm}^{-2}$). This is based on the screened potential U between two colloids [39]: $U = 4\pi\sigma^2 aR \exp(-\kappa d)/(\epsilon\kappa^2(d+a+R))$, with $d = 800 \text{ nm}$ the smallest gap distance between the swimmer and the neighbouring colloids, ϵ and η the permittivity and viscosity of water and $\kappa^{-1} \sim 30 \text{ nm}$ the Debye length in 100 μM salt. The effect of the small spatial variations in absolute $[\text{H}_2\text{O}_2]$ (of order 0.1% [30]) will also be too small to produce the observed oscillations, since swimming speed hardly varies with $[\text{H}_2\text{O}_2]$ at 10% H_2O_2 (Fig. 1b).

We therefore turn to HI and PI. In summary, we will show that for self-electrophoretic swimmers, PI are negligible compared to HI in our geometry; whereas for self-diffusiophoresis, PI and HI make similar contributions. Since recent work shows that self-diffusiophoresis is unlikely to propel these swimmers [30, 31], it is likely that HI dominate. In this case, we find that the swimmer’s flow field is most consistent with that of a pusher, i.e. an extensile flow field. This result can be understood from a simple symmetry argument: an extensile swimmer expels fluid symmetrically fore and aft, which retards the swimmer on approaching a neighbouring colloid, and accelerates it on leaving, Fig. 3a. With 6 neighbouring colloids, this symmetry requires an $\sim 15^\circ$ retardation, close to the experimental value. For the same reason, pullers should show $\delta \sim -15^\circ$, while neutral swimmers (neither pusher nor puller, Fig. 3a) should have $\delta \sim 0^\circ$.

In detail, we model the swimmers as spherical squirmers with a tangential slip velocity u_θ on their surface [40]:

$$u_\theta = 2 \sum_{n=1}^{\infty} \frac{\sin \theta}{n(n+1)} \frac{dP_n(\cos \theta)}{d \cos \theta} B_n, \quad (1)$$

with θ the polar angle ($\theta = 0$ at the polystyrene pole, with flow in the θ direction) and P_n are Legendre polynomials. We take $n \leq 3$ here. The bulk swimming speed

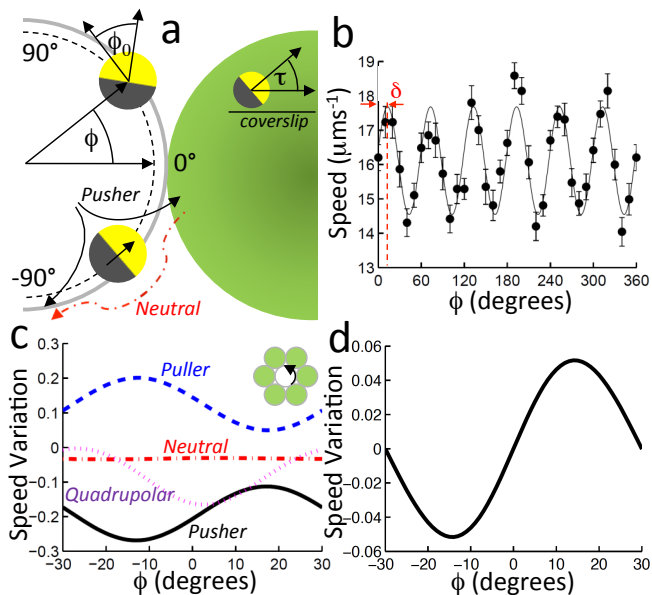


FIG. 3. a) Plan view of Janus swimmer orbiting (dashed line) a central colloid (grey outline) with one neighbouring colloid (solid green). Upper: Definition of angles ϕ , ϕ_0 and (inset) τ . Lower: schematic of flow fields around a pusher (black solid) and a neutral swimmer (red dot-dashed). b) Typical oscillations in orbital speed, from ~ 200 revolutions of a Janus swimmer inside a crystal, in 10% H_2O_2 . Solid curve: 60° Fourier component. c) Predicted relative variation in swimming speed due to HI, for basic swimmers defined in text orbiting a central colloid with six neighbours: pushers (black solid), pullers (blue dashed), neutral squirmers (red dot-dashed), and quadrupolar squirmers (magenta dotted). d) Predicted relative phoretic variation in swimming speed due to the Φ_0 term in Eq. 2, with $\Phi_0 = -2au_0/\mu_p$.

$u_0 = 2B_1/3$ [40]. Defining $b_n = B_n/B_1$, the Stokeslet dipole (the lowest order flow singularity present) is extensile (pusher) if $b_2 < 0$, and contractile (puller) if $b_2 > 0$. Terms with $n > 2$ determine higher order flow fields, with even n giving flow fields with a pusher/puller symmetry, and odd n the symmetry of a neutral swimmer (Fig. 3a).

This surface flow is driven by a generalized phoretic field Φ , here either concentration or electrostatic potential, via: $u_\theta = -\mu_p \partial\Phi/\partial\theta$, which defines the (constant) surface mobility μ_p . In the bulk, $\nabla^2\Phi = 0$, so Φ can be decomposed into spherical harmonics [41]. Matching with Eq. 1 then gives:

$$\Phi = \frac{\Phi_0 a}{r} + \frac{2a}{\mu_p} \sum_{n=1}^{\infty} \frac{B_n}{n(n+1)} \left(\frac{a}{r}\right)^{n+1} P_n(\cos\theta), \quad (2)$$

with r the distance from the swimmer centre. The field Φ generated by a Janus swimmer can also drive electro-diffusio-osmosis on the surface of a static colloid with surface normal $\hat{\mathbf{n}}$ and mobility μ_w , subject to boundary conditions $\hat{\mathbf{n}} \cdot \nabla\Phi = 0$ and $\mathbf{u} = -\mu_w \nabla_{\parallel}\Phi$, where ∇_{\parallel} is the tangential gradient.

The oscillations are determined by how the velocity

and phoretic fields are reflected by the boundary conditions on the neighbouring particles, and how these reflected fields advect the swimmer or drive it phoretically [12, 21, 42]. We approximate interactions between swimmers and each neighbouring colloid by far-field interactions with planes [42] tangent to the colloid at the point on the colloid instantaneously nearest the swimmer. Interactions decaying faster than r^{-3} and secondary reflections with the colloids and glass surface are ignored. In the absence of bulk speed measurements, we assume $u_0 \sim u_g = u_c/1.7$ (see Fig. 1b). For electrophoretic Au-Pt swimmers, theory gives $u_0 \sim 1.2u_g$ [21].

Numerical calculations (detailed in [38]) require several other experimental parameters. From the shadowing effect of the Pt [30, 43], we measured the orientation of the swimmer away from the orbital tangent, in the horizontal (ϕ_0) and, by looking along the plane of the coverslip, vertical (τ) planes, Fig. 3a, finding $\phi_0 = 7 \pm 2^\circ$, and $\tau = 1 \pm 2^\circ$ [38]. We measured a mean orbital radius $\rho = 4.56 \pm 0.02 \mu\text{m}$, giving a swimmer-central colloid gap $g_c \lesssim 200 \text{ nm}$ [38]. We take $g_c = g_p = 70 \pm 10 \text{ nm}$, assuming equidistance of the swimmer from plane (g_p) and colloid. Electrophoretic mobilities (Malvern Zetasizer) in $100 \mu\text{M NaNO}_3$ were $\mu_p = (-5.3 \pm 0.1) \times 10^{-8} \text{ m}^2 \text{ V}^{-1} \text{ s}^{-1}$ and $\mu_w = (-4.4 \pm 0.5) \times 10^{-8} \text{ m}^2 \text{ V}^{-1} \text{ s}^{-1}$. Uncoated Janus particles had $\mu_u = (-5.3 \pm 0.1) \times 10^{-8} \text{ m}^2 \text{ V}^{-1} \text{ s}^{-1}$, justifying the uniform swimmer mobility assumption. We found no oscillations in ϕ_0 and ρ , which are therefore assumed constant.

Considering first purely HI, Fig. 3c shows one period of the speed oscillations calculated for various basic swimmers: pushers ($b_2 = -10$, $b_3 = 0$); pullers ($b_2 = 10$, $b_3 = 0$); neutral squirmers ($b_2 = b_3 = 0$); and quadrupolar squirmers ($b_2 = 0$, $b_3 = 10$). Of these, as expected, only the pusher has retardation ($\delta = 14^\circ$) consistent with experiment. However, the best fit to our data has a quadrupolar component: $b_2 = -15 \pm 7$ and $b_3 = -8 \pm 8$.

Note that, because of the approximations made, these fitted values should only be taken as indicative. However, our symmetry argument should remain valid in the presence of confinement and near-field effects, which do not modify the fore-aft symmetry of the basic flow fields.

Turning to PI, we find [38] that only the first term in Eq. 2 contributes a significant speed oscillation, shown in Fig. 3d. For a self-electrophoretic swimmer, $\Phi_0 = 0$ by charge conservation, because finite Φ_0 implies a current flowing radially outwards from the swimmer. So, for a self-electrophoretic swimmer, the purely hydrodynamic argument above should still apply.

In self-diffusiophoresis, no such conservation law applies, and $\Phi_0 = -2au_0/\mu_p$ [38] for a Janus swimmer. The resulting oscillation (Fig. 3d) with $\delta = 15^\circ$ has the correct retardation, and sufficient amplitude to account for $\sim 50\%$ of the observed oscillations, even for a neutral swimmer. However, as discussed above, self-diffusiophoresis is unlikely in this system.

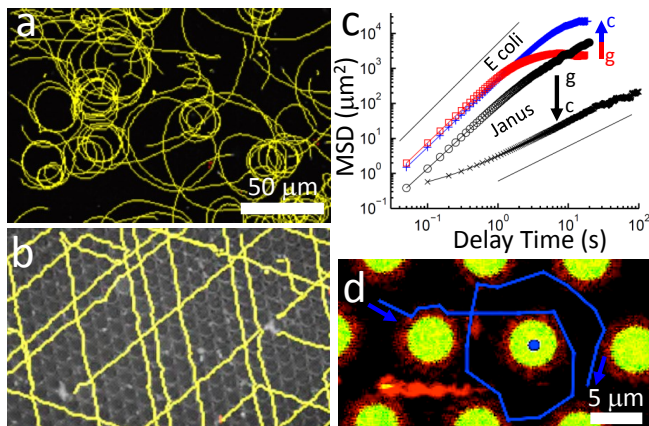


FIG. 4. Tracked videos of smooth-swimming *E. coli* a) on plain glass, and b) inside a crystal. c) MSD on plain glass (\circ = Janus; \square = *E. coli*) and inside the crystal (\times = Janus, $+$ = *E. coli*). Solid lines: diffusive (t) and ballistic (t^2) scaling. Arrows highlight the effect of moving from glass into the crystal ($g \rightarrow c$). d) Confocal microscopy image of a flagella stained (red) bacterium inside a colloidal crystal. Colloids (green) touch each other, but only a small, polar slice is visible. Blue curve: orbital path of a bacterium with shorter flagella (not shown), over 6 seconds.

We therefore conclude that HI dominates orbital speed oscillations in our case. The symmetry and quantitative arguments already outlined, then imply that these Janus swimmers are most consistent with pushers.

However, HI and PI could both be implicated in the net speed-up of swimming inside the crystal (Fig. 1b), and in the stability of the orbital trapping itself. The approximations used so far are invalid for quantifying these effects, because of the swimmer's proximity to the central colloid and the glass surface. Nevertheless, we can still test the suggestion [26] that orbital trapping is due to HI alone.

In purely hydrodynamic trapping, the hopping rate Γ , is determined by a balance between the HI responsible for maintaining a stable swimmer orientation and position, which increase with swimming speed, and thermal fluctuations, which disrupt this stability [26]. Hence, a strong negative correlation between swimming speed and hopping rate should be a signature of purely hydrodynamic trapping. Interestingly, the hopping rate we measure shows no such direct speed dependence. At each $[\text{H}_2\text{O}_2]$, there is a wide variation in u_c , presumably due to Pt surface coating variability, but there is no systematic variation of Γ with u_c : in Fig. 2b, the coloured lines, corresponding to exponential fits through the data for each $[\text{H}_2\text{O}_2]$, are all much flatter than the exponential fit through the mean of each dataset (dashed, black line). Hence, trapping is strongly $[\text{H}_2\text{O}_2]$ dependent (Fig. 2a), but via some speed-independent mechanism. This indicates potential contributions from phoretic effects, as previously discussed theoretically for self-diffusiophoresis

on plane surfaces [12]. However, we can offer no specific explanation for the observed $\Gamma \propto [\text{H}_2\text{O}_2]^{-1}$ dependence.

Finally, we repeat our experiments using motile GFP-labelled smooth-swimming *E. coli* (strain AB1157) in motility buffer [44]. On glass, these bacteria circulate clockwise (viewed from above), Fig. 4a, due to their rotating flagella [33–35]. The crystal rectifies this circulation into straight trajectories, Fig. 4b. The contrast with Janus swimmers is reflected in their mean square displacements (MSD), Fig. 4c. Both swimmers are initially ballistic on plain glass, with the MSD levelling off due to rotational diffusion (Janus swimmers) or circulation (*E. coli*). Within the crystal, Janus swimmers lose their orientational memory by orbiting, leading to diffusive motion, whereas *E. coli*'s rectified trajectories extend the ballistic regime. Hence, the crystal has opposite effects on Janus swimmers and *E. coli*, respectively decreasing and increasing their net diffusivity.

The behavior of *E. coli* can be explained by purely steric effects. Their typical circulation radius (Fig. 4a) is much larger than the inter-colloid spacing, and at $\sim 7 \mu\text{m}$, their flagella are likely to hinder turning out of the straight channels between colloids. Occasionally, bacteria do briefly orbit individual colloids, but imaging *E. coli* with fluorescent flagella [38], shows that these cells typically have shorter, $\sim 3 \mu\text{m}$ flagella (Fig. 4d and SV3 [38]), and so should also have a naturally tighter circulation radius than bacteria with longer flagella [34]. Unlike with the Janus swimmers' orbits, there is no evidence here of interaction with the central colloid, which the bacteria do not approach closely (Fig. 4d).

In conclusion, we have investigated three types of interaction – steric, hydrodynamic and phoretic – between swimmers and the model porous environment of a 2D colloidal crystal. For *E. coli*, the observed rectification of circular orbits into straight trajectories can be explained simply by steric effects, whereas, for Janus swimmers, hydrodynamic and phoretic interactions are important. We find that speed oscillations of synthetic Janus swimmers inside the crystal are consistent with an extensile flow-field around the swimmer. Phoretic effects on these oscillations should be negligible for this swimmer, but may be important for different propulsion mechanisms, or types of swimmer. These conclusions should also be reflected in swimmer-swimmer interactions, with implication for the interpretation of many-body experiments.

Acknowledgements - This work was funded by UK EPSRC grant EP/J007404/1, EU Intra-European Fellowships 623364 LivPaC FP7-PEOPLE-2013-IEF and 623637 DyCoCoS FP7-PEOPLE-2013-IEF, and ERC Advanced Grant ERC-2013-AdG 340877-PHYSAPS. We thank Mike Cates, Elise Darmon, Davide Marenduzzo, Elliot Marsden, Alexander Morozov, Anne Pawsey, Jerko Rosko and Joakim Stenhammar for helpful discussions.

-
- [1] W. C. K. Poon, in *Physics of Complex Colloids*, edited by C. Bechinger, F. Sciortino, and P. Zihlerl (Società Italiana di Fisica, Bologna, 2013) pp. 317–386.
- [2] S. J. Ebbens and J. R. Howse, *Soft Matter* **6**, 726 (2010).
- [3] M. C. Marchetti, J. F. Joanny, S. Ramaswamy, T. B. Liverpool, J. Prost, M. Rao, and R. A. Simha, *Rev. Mod. Phys.* **85**, 1143 (2014).
- [4] Y. Fily and M. C. Marchetti, *Phys. Rev. Lett.* **108**, 235702 (2012).
- [5] J. Stenhammar, A. Tiribocchi, R. J. Allen, D. Marenduzzo, and M. E. Cates, *Phys. Rev. Lett.* **111**, 145702 (2013).
- [6] J. Dunkel, S. Heidenreich, K. Drescher, H. H. Wensink, M. Bär, and R. E. Goldstein, *Phys. Rev. Lett.* **110**, 228102 (2013).
- [7] P. Galajda, J. Keymer, P. Chaikin, and R. Austin, *J. Bact.* **189**, 8704 (2007).
- [8] M. B. Wan, C. J. Olson Reichhardt, Z. Nussinov, and C. Reichhardt, *Phys. Rev. Lett.* **101**, 018102 (2008).
- [9] Y. Hatwalne, S. Ramaswamy, M. Rao, and R. A. Simha, *Phys. Rev. Lett.* **92**, 118101 (2004).
- [10] A. Zöttl and H. Stark, *Phys. Rev. Lett.* **112**, 118101 (2014).
- [11] R. Soto and R. Golestanian, *Phys. Rev. Lett.* **112**, 068301 (2014).
- [12] W. E. Usual, M. N. Popescu, S. Dietrich, and M. Tasinkevych, *Soft Matter* **11**, 434 (2015).
- [13] F. Ginot, I. Theurkauff, D. Levis, C. Ybert, L. Bocquet, L. Berthier, and C. Cottin-Bizonne, *Phys. Rev. X* **5**, 011004 (2015).
- [14] I. Theurkauff, C. Cottin-Bizonne, J. Palacci, C. Ybert, and L. Bocquet, *Phys. Rev. Lett.* **108**, 268303 (2012).
- [15] I. Buttinoni, J. Bialké, F. Kümmel, H. Löwen, C. Bechinger, and T. Speck, *Phys. Rev. Lett.* **110**, 238301 (2013).
- [16] J. Palacci, S. Sacanna, A. P. Steinberg, D. J. Pine, and P. M. Chaikin, *Science* **339**, 936 (2013).
- [17] Q. Liao, G. Subramanian, M. P. DeLisa, D. L. Koch, and M. Wu, *Phys. Fluids* **19**, 061701 (2007).
- [18] K. Drescher, R. E. Goldstein, N. Michel, M. Polin, and I. Tuval, *Phys. Rev. Lett.* **105**, 168101 (2010).
- [19] K. Drescher, J. Dunkel, L. H. Cisneros, S. Ganguly, and R. E. Goldstein, *Proc. Natl Acad. Sci.* **108**, 10940 (2011).
- [20] J. S. Guasto, K. A. Johnson, and J. P. Gollub, *Physical review letters* **105**, 168102 (2010).
- [21] T.-Y. Chiang and D. Velegol, *Langmuir* **30**, 2600 (2014).
- [22] K. Ishimoto and E. A. Gaffney, *Phys. Rev. E* **88**, 062702 (2013).
- [23] G. Li and J. X. Tang, *Phys Rev Lett* **103**, 078101 (2009).
- [24] G.-J. Li and A. M. Ardekani, *Phys. Rev. E* **90**, 013010 (2014).
- [25] G.-J. Li, A. Karimi, and A. Ardekani, *Rheologica Acta* **53**, 911 (2014).
- [26] D. Takagi, J. Palacci, A. B. Braunschweig, M. J. Shelley, and J. Zhang, *Soft Matter* **10**, 1784 (2014).
- [27] G. Volpe, I. Buttinoni, D. Vogt, H.-J. Kümmerer, and C. Bechinger, *Soft Matter* **7**, 8810 (2011).
- [28] J. R. Howse, R. A. L. Jones, A. J. Ryan, T. Gough, R. Vafabakhsh, and R. Golestanian, *Phys. Rev. Lett.* **99**, 048102 (2007).
- [29] S. Ebbens, M.-H. Tu, J. R. Howse, and R. Golestanian, *Phys. Rev. E* **85**, 020401 (2012).
- [30] A. T. Brown and W. C. K. Poon, *Soft Matter* **10**, 4016 (2014).
- [31] S. Ebbens, D. A. Gregory, G. Dunderdale, J. R. Howse, Y. Ibrahim, T. B. Liverpool, and R. Golestanian, *Euro. Phys. Lett.* **106**, 58003 (2014).
- [32] W. F. Paxton, K. C. Kistler, C. C. Olmeda, A. Sen, S. K. St. Angelo, Y. Cao, T. E. Mallouk, P. E. Lammert, and V. H. Crespi, *J. Am. Chem. Soc.* **126**, 13424 (2004).
- [33] M. A.-S. Vigeant, R. M. Ford, M. Wagner, and L. K. Tamm, *Appl. Environ. Microbiol.* **68**, 2794 (2002).
- [34] E. Lauga, W. R. DiLuzio, G. M. Whitesides, and H. A. Stone, *Biophys. J.* **90**, 400 (2006).
- [35] H. Shum, E. A. Gaffney, and D. J. Smith, *Proc. Royal Soc. A* **466**, 1725 (2010).
- [36] A. I. Campbell and S. J. Ebbens, *Langmuir* **29**, 14066 (2013).
- [37] J. C. Crocker and D. G. Grier, *J. Colloid Interface Sci.* **179**, 298 (1996).
- [38] See online supplementary material at [http://. .](http://.)
- [39] M. Leunissen, C. Christova, A.-P. Hynninen, C. Royall, A. Campbell, A. Imhof, M. Dijkstra, R. Van Roij, and A. Van Blaaderen, *Nature* **437**, 235 (2005).
- [40] M. J. Lighthill, *Comm. Pure Appl. Maths* **5**, 109 (1952).
- [41] R. Golestanian, T. B. Liverpool, and A. Ajdari, *New J. Phys.* **9**, 126 (2007).
- [42] S. E. Spagnolie and E. Lauga, *J. Fluid Mech.* **700**, 105 (2012).
- [43] S. J. Ebbens and J. R. Howse, *Langmuir* **27**, 12293 (2011).
- [44] I. D. Vladescu, E. J. Marsden, J. Schwarz-Linek, V. A. Martinez, J. Arlt, A. N. Morozov, D. Marenduzzo, M. E. Cates, and W. C. K. Poon, *Phys. Rev. Lett.* **113**, 268101 (2014).

Swimming in a Crystal: Hydrodynamic, Phoretic and Steric Interactions Supplementary Material

Aidan T. Brown,¹ Ioana D. Vladescu,¹ Angela Dawson,¹ Teun Vissers,¹

Jana Schwarz-Linek,¹ Juho S. Lintuvuori,^{1,2} and Wilson C. K. Poon¹

¹*SUPA, School of Physics and Astronomy, The University of Edinburgh,
King's Buildings, Peter Guthrie Tait Road, Edinburgh, EH9 3FD, United Kingdom*

²*Laboratoire de Physique des Solides, Université Paris-Sud, UMR 8502 - 91405 Orsay, France*

SUPPLEMENTARY VIDEO INFORMATION

SV1 - Janus swimmers moving through a colloidal crystal in 1% H₂O₂. Epifluorescence, at 3 fps, 50 μm scale bar.

SV2 - High magnification video of a Janus swimmer orbiting a single colloid inside a crystal at 10% H₂O₂. Epifluorescence (initially brightfield to show location of neighbouring colloids) at 20 fps, 5 μm scale bar.

SV3 - Confocal video of *E. coli* bacteria with green stained bodies and red stained flagella swimming inside a colloidal crystal (green). Colloids touch each other, but only small, polar end caps are visible. Early in the video, an *E. coli* with short flagella orbits the colloid marked with a blue circle. 4 fps, 10 μm scale bar.

SV4 - High magnification, edge-on video of a Janus swimmer orbiting a single colloid at the edge of a crystal in 10% H₂O₂. Epifluorescence at 20 fps, 5 μm scale bar.

GEOMETRICAL MEASUREMENTS

In this section, we give details of how we estimate the gap sizes and inclination angles between the surface of the swimmer, and the static colloid and glass surfaces.

As the swimmer orbits a single colloid, we wish to measure the radius ρ of its orbit, the azimuthal angle of the swimmer around its orbit ϕ , and the inclination ϕ_0 and τ of the swimmer's orientation away from the tangent to that orbit (see Fig. S1c). However, since the Janus particle has non-uniform fluorescence intensity, we cannot straightforwardly determine the centre of the particle. We instead measure equivalent parameters (ρ' , ϕ' , ϕ'_0) for an ellipse fitted to a thresholded image of the swimmer at each frame, whose centre will be offset from the true centre of the swimmer by some small distance Δc along the swimmer's orientation vector.

The expected shape of the image of the swimmer is not clear, since the Pt coating appears to only partially block out the underlying fluorescence (see supplementary video SV2). We estimate Δc from the aspect ratio of the fitted ellipse by performing identical ellipse fitting in MATLAB

on two models of the changing thresholded shape of the swimmer which have the lower half of the image either a half-ellipse or a truncated semicircle (Fig. S1a).

We plot the relationship between the difference ΔL in the fitted major and minor axis lengths, and the offset of the centroid Δc in these two models, and use the average of these two curves to estimate the experimental value of Δc . The radius of the Janus swimmers is $a = 0.96 \pm 0.04$ μm, and, averaging over 17 videos, we find $\Delta L = 360 \pm 20$ nm, giving $\Delta c = 135 \pm 30$ nm, where the difference between the two curves in Fig. S1a has been taken into account in the uncertainty. To lowest order in Δc , the corrections to ρ , ϕ and ϕ_0 are then given by:

$$\begin{aligned}\rho &= \rho' - \Delta c \langle \sin \phi'_0 \rangle, \\ \phi &= \phi' - \frac{\Delta c}{\langle \rho' \rangle} \langle \cos \phi'_0 \rangle,\end{aligned}\quad (\text{S1})$$

$$\phi_0 = \phi'_0 - \frac{\Delta c}{\langle \rho' \rangle} \langle \cos \phi'_0 \rangle.$$

The corrections are approximately 20 nm, and 2° respectively, and these have already been applied here and in the main text, to give $\langle \rho \rangle = 4.56 \pm 0.02$ μm and $\langle \phi_0 \rangle = 7 \pm 2^\circ$.

From the average value of the orbital radius $\langle \rho \rangle$, we calculate the size of the gaps between the swimmer surface and the static colloid g_c or the plane glass surface g_p . The geometric construction in Fig. S1b gives the following expression for g_c and g_p

$$\rho^2 + (R - g_p - a)^2 = (R + g_c + a)^2, \quad (\text{S2})$$

where the radius of the static colloids, $R = 5.06 \pm 0.02$ μm, and the averages $\langle \dots \rangle$ has been dropped for convenience. This single equation cannot be used to solve for both g_c and g_p . However, since both gap sizes must be positive, we can obtain upper bounds on each:

$$\begin{aligned}g_p &< \frac{\rho^2 - 4Ra}{2(R - a)}, \\ g_c &< \frac{\rho^2 - 4Ra}{2(R + a)},\end{aligned}\quad (\text{S3})$$

where we have ignored small terms quadratic in g_p , g_c . Calculating these limits gives $g_c < 200$ nm and $g_p < 300$

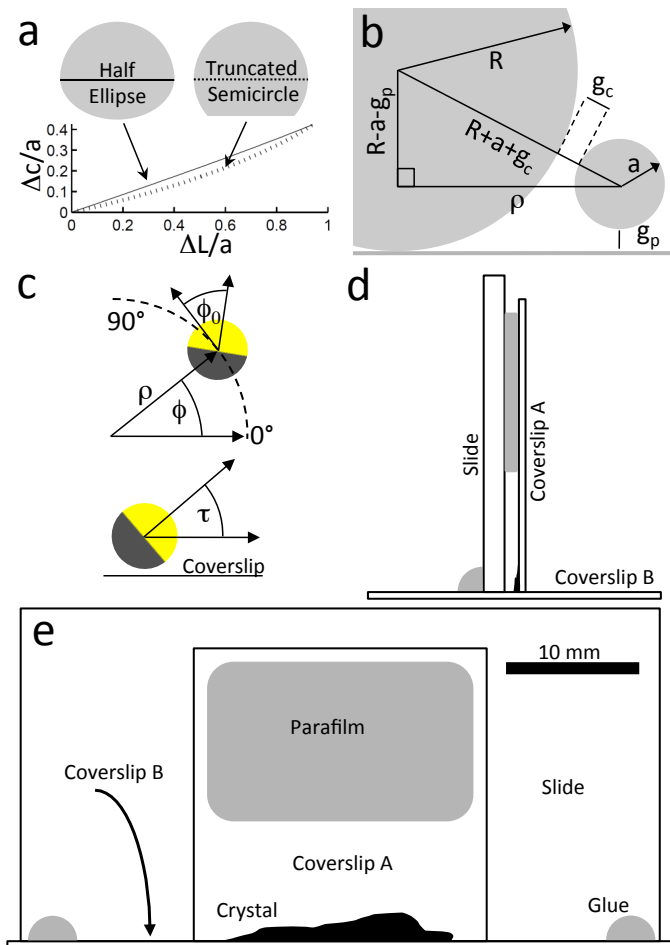


FIG. S1. a) Results of estimating the offset of a fitted ellipse $\Delta c/a$ from the difference in fitted axis lengths $\Delta L/a$ based on two models shown here and described in the text. b) Side view of a swimmer orbiting a colloid (not to scale) with geometrical construction to determine the size of the gaps g_c and g_p between the swimmer and the colloid or plane. c) Plan and side views of a Janus swimmer defining ρ , ϕ , ϕ_0 and τ . $\phi = 0$ is defined as the angle to one of the neighbouring colloids. d-e) Diagrams of the sample cell for observation along the plane of the coverslip. Observation is from below coverslip B, through the crystal and along the plane of coverslip A.

nm, taking the largest value within experimental error. If instead, we assume that $g_c = g_p = g$, Eq. S2 gives:

$$g = \frac{\rho^2}{4R} - a, \quad (\text{S4})$$

or $g = 70 \pm 10$ nm.

To obtain the inclination τ w.r.t. the glass plane (Fig. S1c), 10 Janus swimmers orbiting colloids in the crystal were observed along the plane of the coverslip using a custom-built sample chamber, shown in Fig. S1d-e. A colloidal crystal was formed at the edge of a 22×22 mm² coverslip (A), as in the main text. Coverslip A was attached with ~ 600 μm parafilm to a glass slide previously cut down to 50 mm, so that the edge of coverslip A

was flush with the long edge of the slide, with the crystal facing inwards. The slide was then glued onto a 22×50 mm² coverslip (B), the crystal lying next to coverslip B. Janus swimmers in 10% H₂O₂ solution were added as usual, and viewed through coverslip B using a $100\times$ oil immersion objective. Swimmers were recorded orbiting single colloids at the lower edge of the crystal, and images were captured with a CoolSNAP (Photometrics) camera using MicroManager [1] (see SV4). The inclination $\tau = 1 \pm 2^\circ$ of the swimmers w.r.t. coverslip A was determined by fitting ellipses to thresholded images of the swimmers, as above.

SPEED OSCILLATIONS

We present in this section details of the approximate calculation of the hydrodynamic and phoretic interactions between a swimmer following a circular orbit, and a ring of static colloids outside that orbit. The approach we use is to write down the velocity and phoretic fields generated by a swimmer in free space, and from these determine the additional reflected fields necessary to match boundary conditions on the static colloids. These reflected fields then advect the swimmer, and move it phoretically, producing speed oscillations as the distance between the swimmer and neighboring colloids varies around the swimmer's orbit. As in [2, 3], we consider only the first reflected fields, and ignore secondary reflections from the swimmer and from other boundaries, including the central colloid and the glass slide.

We make the further approximation of replacing the spherical boundaries of the static colloids by planes tangent to each colloid at the instantaneous point of closest approach between colloid and swimmer. This allows us to use analytical results for the far-field interaction between swimmers and planes [2]. This approach can be justified here by noting that the shortest distance between the swimmer and the nearest colloid is ~ 800 nm, similar to the swimmer's radius. It is therefore large enough that the far-field approximations will be at least qualitatively correct, as determined by numerical calculations in [2], yet much smaller than the size of the static colloid, so that the planar approximation is also reasonable.

Hydrodynamic effects

We will deal first with the hydrodynamic interactions alone, assuming the usual non-slip boundary conditions at the static colloid surfaces, and ignoring phoretic effects, which we add later.

In free space, the far-field flow around the squirmer can be broken up into a series of singularity solutions. With the squirmer positioned at the origin, and axisymmetric along a vector $\hat{\mathbf{v}}$, which is also the swimming direction,

we list the lowest order axisymmetric components [4]. Defining $\cos \theta = \hat{\mathbf{v}} \cdot \hat{\mathbf{r}}$, and $\hat{\mathbf{r}}$ and $\hat{\theta}$ as the unit vectors in the radial and θ directions, these are the Stokeslet:

$$\mathbf{G} = \frac{1}{r} \left[2 \cos \theta \hat{\mathbf{r}} - \sin \theta \hat{\theta} \right], \quad (\text{S5})$$

the stresslet:

$$\mathbf{S} = \frac{1}{2r^2} (1 + 3 \cos 2\theta) \hat{\mathbf{r}}, \quad (\text{S6})$$

the Stokes quadrupole:

$$\mathbf{Q} = \frac{1}{r^3} \left[(\cos \theta + 3 \cos 3\theta) \hat{\mathbf{r}} + \frac{1}{4} (3 \sin 3\theta - \sin \theta) \hat{\theta} \right], \quad (\text{S7})$$

and the source dipole:

$$\mathbf{P}_D = \frac{1}{r^3} \left[2 \cos \theta \hat{\mathbf{r}} + \sin \theta \hat{\theta} \right]. \quad (\text{S8})$$

As in [2], the undisturbed flow field around the swimmer can be written as:

$$\mathbf{u} = \alpha \mathbf{S} + \beta \mathbf{P}_D + \gamma \mathbf{Q} + \dots, \quad (\text{S9})$$

where terms decaying as r^{-4} and faster are not included, and there is no Stokeslet component because the swimmer is force free.

We then specify the spatial relationship of the swimmer and the neighbouring colloids. The swimmer is centred at \mathbf{s} , with a neighbouring colloid fixed at \mathbf{X} . While the swimmer is axisymmetric w.r.t. the direction $\hat{\mathbf{v}}$, and would swim along that direction in free space, the swimmer is here constrained to follow a circular orbit, whose tangent vector is $\hat{\mathbf{p}}$. In general, $\hat{\mathbf{v}} \neq \hat{\mathbf{p}}$. The displacement vector \mathbf{l} of the swimmer from the static colloid is $\mathbf{l} = \mathbf{s} - \mathbf{X}$, with centre-to-centre distance $l = |\mathbf{l}|$. The radius of the large colloid is R , and $h = l - R$ is the distance between the centre of the swimmer and the surface of the neighbouring colloid.

We decompose the swimmer's orientation into components perpendicular and parallel to the static colloid's surface, in order to use the expressions for the advected velocity given in [2]. The unit vector $\hat{\mathbf{l}} = \mathbf{l}/l$ points along \mathbf{l} , while $\hat{\mathbf{k}} = \hat{\mathbf{l}} \times (\hat{\mathbf{v}} \times \hat{\mathbf{l}})/|\hat{\mathbf{v}} \times \hat{\mathbf{l}}|$, is parallel to the colloid surface, and in the $\hat{\mathbf{v}}, \hat{\mathbf{l}}$ plane. In this coordinate system:

$$\hat{\mathbf{v}} = \hat{\mathbf{k}} \cos \sigma + \hat{\mathbf{l}} \sin \sigma, \quad (\text{S10})$$

where σ is the inclination of the swimmer away from the tangent plane to the colloid's surface. Hence, $\sin \sigma = \hat{\mathbf{v}} \cdot \hat{\mathbf{l}}$. We define two other angles likewise: $\sin \psi = \hat{\mathbf{p}} \cdot \hat{\mathbf{l}}$, and $\cos \chi = \hat{\mathbf{p}} \cdot \hat{\mathbf{v}}$.

The hydrodynamic interactions between a free swimmer, moving originally at speed u_0 along direction $\hat{\mathbf{v}}$, and the tangent plane, would in general result in an additional

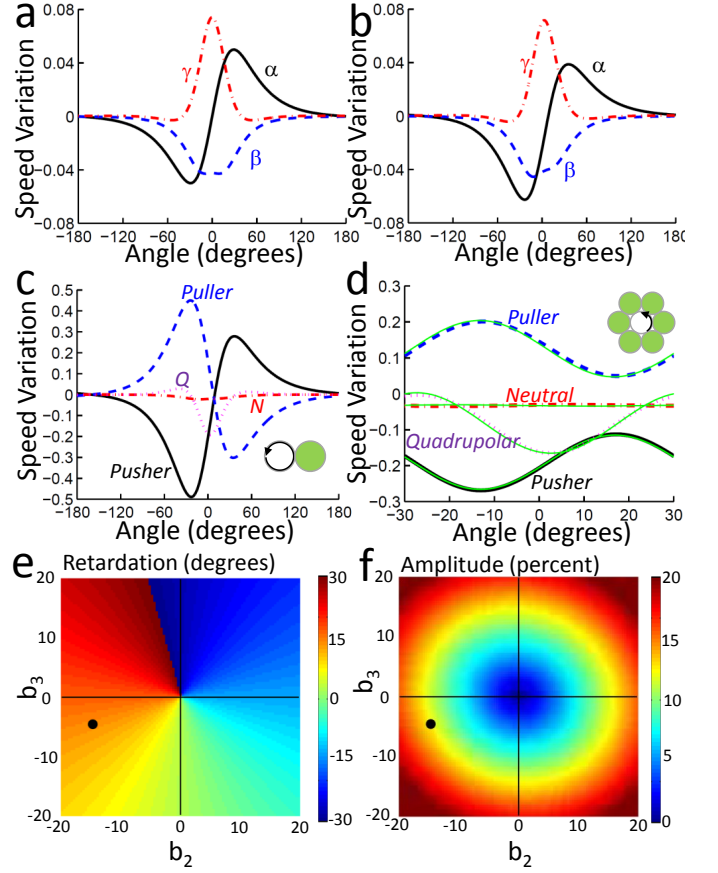


FIG. S2. a) Contribution to the swimming speed made by unit amplitude Stokeslet dipole (α , black solid), source dipole (β , blue dashed) and Stokeslet quadrupole (γ , red dot-dashed) components, for $\phi_0 = \tau = 0$, and a single neighbouring colloid at $\phi = 0$. b) As in a), but with $\phi_0 = 7^\circ$, $\tau = 1^\circ$, as found experimentally. c) Fractional variation in swimming speed produced by swimmers orbiting a central colloid with a single neighbour at $\phi = 0$, for a set of swimmers defined in text: pushers (black solid), pullers (blue dashed), neutral squirmers (red dot-dashed), and quadrupolar squirmers (magenta dotted). ϕ_0 , τ and ρ are set at experimental values, with the swimmer equidistant from the colloid and plane: $g_c = g_p = 70$ nm. d) As in c), but with 6 neighboring colloids (inset). Solid, green lines: 60° Fourier component. e-f) Maps of the retardation (e) and fractional amplitude (f) of the fitted oscillation as a function of b_2 and b_3 . Colourbars are in degrees and percent respectively, and \bullet indicates the best fit values of b_2 , b_3 for the experimental retardation and amplitude.

swimmer velocity $\Delta \mathbf{u}$, which can be decomposed along $\hat{\mathbf{l}}$ and $\hat{\mathbf{k}}$:

$$\Delta \mathbf{u} = u_l(h, \sigma, u_0) \hat{\mathbf{l}} + u_k(h, \sigma, u_0) \hat{\mathbf{k}}. \quad (\text{S11})$$

In the present case, however, the particle velocity is constrained to lie on the tangent, $\hat{\mathbf{p}}$, so the observed variation in swimmer speed will be $u' = \hat{\mathbf{p}} \cdot \Delta \mathbf{u}$, or:

$$u' = u_l \sin \psi + u_k \frac{\cos \chi - \sin \psi \sin \sigma}{\cos \sigma}, \quad (\text{S12})$$

where, for the velocity components u_l and u_k , we use the

far-field interaction formulae given in [2]. Translating into our coordinate system, these are:

$$\begin{aligned} u_l &= \frac{-3\alpha(1-3\sin^2\sigma)}{8h^2} - \frac{\sin\sigma}{4h^3} \left[4\beta + \gamma(9\sin^2\sigma - 7) \right] \\ u_k &= \frac{3\alpha\sin(2\sigma)}{8h^2} - \frac{\cos\sigma}{16h^3} \left[4\beta + \gamma(27\sin^2\sigma - 7) \right]. \end{aligned} \quad (\text{S13})$$

We then express the flow field coefficients (α, β, γ) , as functions of the surface flow on the squirmer. We consider a spherical squirmer of radius a with a tangential slip velocity profile given by [5]:

$$\mathbf{u}_\theta(r=a) = 2 \sum_{n=1}^{\infty} \frac{\sin\theta}{(n+1)n} \frac{dP_n(\cos\theta)}{d\cos\theta} B_n, \quad (\text{S14})$$

where θ is the polar angle ($\theta = 0$ at the PS pole, and flow is in the θ direction) and P_n are Legendre polynomials. For simplicity, we consider only $n \leq 3$. The bulk self propulsion speed is $u_0 = 2B_1/3$ [5]. B_2 determines whether the Stokeslet dipole (the lowest order flow singularity present) is extensile (pusher, $B_2 < 0$) or contractile (puller, $B_2 > 0$). Following [6], we define $b_n = B_n/B_1$. In [6], the connection is made between the far-field flow components, and the slip velocity components:

$$\begin{aligned} \alpha &= -(3/4)a^2b_2u_0, \\ \beta &= (1/2 - b_3/8)a^3u_0, \\ \gamma &= (-5b_3/16)a^3u_0, \end{aligned} \quad (\text{S15})$$

and combining Eq. S12, S13, S15 then gives the predicted fractional speed variation $\tilde{u}_0 = u'/u_0$.

We now calculate the interaction between our swimmer and a single neighbouring colloid. The glass surface is on the $x-y$ plane, with z pointing into the sample. The origin is at the point of contact between the central colloid and the plane. We take the swimmer to be a small distance g_p above the glass plane, and orbiting at horizontal distance ρ from the z -axis through the centre of the central colloid ($x = y = 0$), and define its position \mathbf{s} in terms of the azimuthal angle ϕ :

$$\mathbf{s} = (\rho \cos\phi, \rho \sin\phi, a + g_p). \quad (\text{S16})$$

The neighbouring colloid is fixed at:

$$\mathbf{X} = (2R, 0, R), \quad (\text{S17})$$

while the tangent to the circular orbit of the swimmer is:

$$\hat{\mathbf{p}} = (-\sin\phi, \cos\phi, 0), \quad (\text{S18})$$

and the orientation of the swimmer is:

$$\hat{\mathbf{v}} = (-\sin(\phi - \phi_0)\cos\tau, \cos(\phi - \phi_0)\cos\tau, \sin\tau), \quad (\text{S19})$$

where ϕ_0 is the fixed angle between the tangent to the orbit and the orientation of the swimmer in the $x-y$ plane, and τ is the fixed inclination of the swimmer away from the horizontal plane (Fig. S1c). This gives $\cos\chi = \cos\phi_0\cos\tau$.

In Fig. S2a-b we plot the speed oscillation contribution from each of the flow singularities, for a swimmer with a single neighbouring colloid. We take the experimental parameters: $a = 0.96 \mu\text{m}$, $R = 5.06 \mu\text{m}$, $\rho = 4.56 \mu\text{m}$ and $g_p = 70 \text{ nm}$ (so that the swimmer is equidistant from colloid and plane). In a), we set $\phi_0 = \tau = 0$, whereas in b), we use the experimental values: $\phi_0 = 7^\circ$, $\tau = 1^\circ$. This allows one to see the symmetry of each contribution. In a), the pusher-puller mode (α) is the only mode which is odd about the origin, and therefore the only mode which could result in the close to 15° retardation seen experimentally. Taking into account the non-zero inclination of the swimmer to the tangent (Fig. S2b), these modes lose their symmetry slightly.

The total squirmer flow field always contains a fixed B_1 contribution, and variable contributions from the two other modes, B_2 and B_3 according to Eq. S15. In Fig. S2c, we plot the fractional speed variation produced by four basic swimmers. These are pushers ($b_2 = -10$, $b_3 = 0$), pullers ($b_2 = 10$, $b_3 = 0$), neutral squirmers ($b_2 = b_3 = 0$) and quadrupolar squirmers ($b_2 = 0$, $b_3 = 10$). The pusher accelerates as it passes closest to the neighbouring colloid, at $\phi = 0$, whereas the puller slows down. As discussed in the main text, this is as expected, considering the extensile and contractile flow fields around the two swimmers. The neutral and quadrupolar swimmers, on the other hand, show approximately symmetrical behaviour around $\phi = 0$, in line with the symmetry of the source dipole and Stokeslet quadrupole (β, γ) flow components, which are the only components contributing to the flow fields of these swimmers.

To calculate the interaction between the swimmer and multiple spheres, we add the contributions from single spheres located at 60° intervals around the central axis. In Fig. S2d, we plot the speed oscillations produced by six neighbouring colloids for the same set of swimmers. All of the oscillations are well described by sinusoids with period 60° , but the retardation and amplitude of the oscillation depends on the type of swimmer: the pusher matches the experimentally observed retardation of $\sim 15^\circ$, whereas the puller has a retardation of $\sim -15^\circ$, and the other swimmers retardation close to 0° and 30° . Fig. S2e-f show the retardation and fractional amplitude variation of this 60° period oscillation as a function of b_2 and b_3 .

The fractional amplitude calculated here is $\tilde{u}_0 = u'/u_0$, whereas experimentally, we measure $\tilde{u} = u'/u_c$ where u_c is the average swimming speed in the crystal. Assuming $u_0 = u_g$, the swimming speed on plain glass, we require $\tilde{u}_0 = 13 \pm 2\%$ to match experimental values (us-

ing the experimental values of $u_c/u_g = 1.7 \pm 0.3$ and $\tilde{u} = 7.7 \pm 0.5\%$). The best fit for the experimentally observed amplitude and retardation is then $b_2 = -15 \pm 7$, $b_3 = -5 \pm 6$, where the uncertainty is estimated from the experimental uncertainty in each input parameter.

Phoretic effects

We now consider the effect of the phoretic fields (concentration, electrostatic potential, etc.) which propel the swimmer. These phoretic fields, by interacting with another surface (a single neighbouring colloid, approximated as a plane), can modify the speed of the swimmer in two ways: (i) the phoretic field, reflected from this surface, moves the swimmer by (diffusio- or electro-) phoresis, and (ii) the phoretic field drives an osmotic fluid flow tangent to the surface, and this fluid flow advects the swimmer.

Under the approximations used for the hydrodynamic calculations, it is simple to calculate the direct effect of the reflected phoretic fields (i), but the osmotic effect (ii) is more difficult, as the no-slip boundary conditions on the fluid velocity no longer apply. We will solve this problem by artificially splitting the velocity field into two components: one which matches the osmotic boundary conditions on the surface; and one which has no-slip boundary conditions. Considering only the first reflection from a single surface, as above, these two flow fields can then be determined separately, and the speed modification calculated.

We find that the result of this calculation depends on whether we are considering electrophoresis or diffusiophoresis. For a diffusiophoretic swimmer, the only significant phoretic contribution (combining i and ii) is an oscillation with a retardation of 15° , and a similar amplitude to the experimental oscillations, which derives from the net concentration flux through the swimmer surface. For an electrophoretic swimmer, however, charge conservation means there is no such net flux term, so the phoretic contribution to the speed oscillation is insignificant.

We first write down the bulk equations obeyed by the flow \mathbf{u} and phoretic fields Φ , and their boundary conditions on the neighbouring surface. In the bulk, the fluid velocity obeys the continuity equation $\nabla \cdot \mathbf{u} = 0$, and the Stokes equation:

$$\eta \nabla^2 \mathbf{u} = -\nabla p, \quad (\text{S20})$$

with η the fluid viscosity and p the hydrostatic pressure, while the phoretic field obeys $\nabla^2 \Phi = 0$.

We here make the common Smoluchowski approximation that the phoretic slip length is much smaller than other lengthscales, so that phoretic effects just modify the boundary conditions on the neighbouring surface, which

are:

$$\mathbf{u} = -\mu_w \nabla_{\parallel} \Phi, \quad (\text{S21})$$

with μ_w the phoretic mobility of this surface. Here, the surface gradient, $\nabla_{\parallel} = (\mathbb{I} - \hat{\mathbf{n}}\hat{\mathbf{n}}) \cdot \nabla$, with $\hat{\mathbf{n}}$ the surface normal pointing into the fluid and \mathbb{I} the identity operator.

Meanwhile, the boundary condition on the phoretic field is:

$$\hat{\mathbf{n}} \cdot \nabla \Phi = 0. \quad (\text{S22})$$

In the case of a concentration field, this is because there must be no flux of chemical species through this boundary, whereas for the electrostatic potential, this boundary condition is approximately correct because the electric permittivity ϵ is much smaller inside the colloid than in the fluid. Because we are only considering the first reflection, from a single boundary, we do *not* enforce the equivalent boundary conditions on the swimmer.

We note that it is these two boundary conditions on the neighbouring colloid which give rise to the two separate effects of the phoretic field. The direct effect of the reflected field (i) comes from Eq. S22, while the induced osmotic flow effect (ii) comes from Eq. S21.

To calculate the flow fields, we will extend the method of [7], and artificially decompose the fluid velocity into two components: $\mathbf{u} = \mathbf{u}_p + \mathbf{u}_q$, where \mathbf{u}_p is the potential flow field given by:

$$\mathbf{u}_p = -\mu_w \nabla \Phi. \quad (\text{S23})$$

Because there is no normal phoretic field at the surface (Eq. S22), \mathbf{u}_p satisfies the osmotic boundary condition Eq. S21 on its own, so that the remaining field \mathbf{u}_q must satisfy a no-slip boundary condition. Similarly, $\nabla^2 \mathbf{u}_p = 0$, so \mathbf{u}_q must also satisfy Stokes equation, Eq. S20 on its own. Hence, we can treat \mathbf{u}_q exactly as a normal flow-field around the swimmer, with no-slip boundary conditions on the neighbouring surface, just as in the previous section, while \mathbf{u}_p is entirely determined by Eq. S23.

This separation is only possible because we only consider the first reflection from a neighbouring surface of constant mobility. Otherwise, we would have to match the boundary condition on the swimmer, or on other surfaces of differing mobility, and these could not be satisfied by a single function like \mathbf{u}_p in Eq. S23.

We can write each of these potential (Φ) and flow (\mathbf{u} , \mathbf{u}_p , \mathbf{u}_q) fields as sums of an undisturbed (labelled 0), and an image (labelled *) field, chosen so as to match the boundary conditions Eq. S21-S22, i.e. $\Phi = \Phi^0 + \Phi^*$ etc. We have enough freedom to also demand:

$$\begin{aligned} \mathbf{u}^0 &= \mathbf{u}_p^0 + \mathbf{u}_q^0, \\ \mathbf{u}^* &= \mathbf{u}_p^* + \mathbf{u}_q^*, \end{aligned} \quad (\text{S24})$$

and, to satisfy Eq. S23:

$$\begin{aligned} \mathbf{u}_p^0 &= -\mu_w \nabla \Phi^0, \\ \mathbf{u}_p^* &= -\mu_w \nabla \Phi^*, \\ \mathbf{u}_q^0 &= \mathbf{u}^0 + \mu_w \nabla \Phi^0, \end{aligned} \quad (\text{S25})$$

with \mathbf{u}_q^* left to be determined from the no-slip boundary condition on \mathbf{u}_q .

The total modification in particle speed u^T produced by the boundary is then given by phoresis in the image field (i), and advection by the image velocity (ii):

$$u^T = \hat{\mathbf{p}} \cdot (\mu_p \nabla \Phi^* + \mathbf{u}^*)_{\mathbf{r}=\mathbf{s}}, \quad (\text{S26})$$

with μ_p the swimmer's phoretic mobility, here assumed constant. The fields are evaluated at the position $\mathbf{r} = \mathbf{s}$ of the swimmer centre, and the dot product with $\hat{\mathbf{p}}$ again comes from the orbital constraint. We write u^T as $u^T = u' + u''$, where u' is the speed variation due to pure hydrodynamics (as calculated above), and u'' is the additional speed variation. Using the identities above:

$$u'' = \hat{\mathbf{p}} \cdot [(\mu_p - \mu_w) \nabla \Phi^* + \mathbf{u}_q^*]_{\mathbf{r}=\mathbf{s}} - u'. \quad (\text{S27})$$

Note that this mathematical formalism has blurred the identities of the two physical contributions (i and ii). The first term in Eq. S27, which looks purely phoretic, includes a contribution $(-\mu_w \nabla \Phi^*)$, which really comes, through Eq. S23, from the flow field around the swimmer.

To determine the first part of the speed variation in Eq. S27, we write the undisturbed phoretic field Φ^0 as a

function of spherical harmonics, as in [8]:

$$\Phi^0 = \Phi_0^0 \frac{a}{|\mathbf{r} - \mathbf{s}|} + \frac{2a}{\mu_p} \sum_{n=1}^{\infty} \frac{B_n}{n(n+1)} \left(\frac{a}{|\mathbf{r} - \mathbf{s}|} \right)^{n+1} P_n(\cos \theta), \quad (\text{S28})$$

where $\cos \theta = \hat{\mathbf{v}} \cdot (\mathbf{r} - \mathbf{s})/|\mathbf{r} - \mathbf{s}|$ because the swimmer points along $\hat{\mathbf{v}}$. The coefficients of each spherical harmonic come from the definition of the surface flow components B_n in Eq. S14, combined with the undisturbed tangential flow u_θ on the squirmer's surface:

$$u_\theta = -\mu_p \frac{d\Phi^0}{d\theta}, \quad (\text{S29})$$

where only the first coefficient Φ_0^0 remains to be determined, as this harmonic does not contribute to the slip velocity. The image field Φ^* which satisfies the boundary condition Eq. S22 on the plane tangent to the neighbouring colloid, is then simply a reflection of Φ^0 across this plane.

To determine the second part of the speed variation, we repeat the calculations for a pure squirmer from the previous section, but replace the undisturbed velocity field \mathbf{u}^0 with the field \mathbf{u}_q^0 defined in Eq. S25. Keeping terms only up to order h^{-3} , this modified flow field contains, in addition to the original flow field, a source dipole term, and a source term $\mathbf{J} = r^{-2} \hat{\mathbf{r}}$:

$$\mathbf{u}_q^0 = \mathbf{u}^0 - \mu_w \Phi_0^0 a \mathbf{J} - \frac{3a^3 u_0 \bar{\mu}}{2} \mathbf{P}_D + \dots \quad (\text{S30})$$

where $\bar{\mu} = \mu_w / \mu_p$. Note that there is no real source term in the far-field flow around the swimmer, but that this is a result of the blurring of physical effects discussed above. The effect of a source term of strength δ is to push the swimmer away from the wall with speed $(3/4)\delta h^{-2}$ [9], here along the $\hat{\mathbf{l}}$ direction. Evaluating the advection of the swimmer due to Eq. S30, as in the previous section, gives the second part of Eq. S27, and we then obtain for the total phoretic speed variation:

$$u'' = -\frac{a\mu_p \Phi_0^0 \sin \psi}{4h^2} (1 + 2\bar{\mu}) + \frac{3a^3 u_0}{16h^3} [(\bar{\mu} + 1) \cos \chi + (5\bar{\mu} + 1) \sin \sigma \sin \psi] + \dots, \quad (\text{S31})$$

where terms decaying faster than h^{-3} have been excluded. We note without proof that, even if such terms are included, the total phoretic contribution (i and ii) from a particular b_n component, for $n > 1$, decays as $h^{-(n+2)}$, whereas the equivalent purely hydrodynamic contribution decays as h^{-n} , so that, in general, apart from the contributions written out explicitly in Eq. S31, the phoretic effects will make a negligible contribution com-

pared to pure hydrodynamics.

For an electrophoretic swimmer, $\Phi_0^0 = 0$ due to charge conservation, since this lowest harmonic corresponds to a finite current flowing radially outward from the swimmer. To calculate the predicted oscillations of an electrophoretic swimmer, we measured the electrophoretic mobilities of the Janus swimmers and the static colloids in 100 μM NaNO_3 using a Malvern Ze-

tasizer, finding for the Janus swimmers, $\mu_p = (-5.3 \pm 0.1) \times 10^{-8} \text{m}^2 \text{V}^{-1} \text{s}^{-1}$ and for the static colloids, $\mu_w = (-4.4 \pm 0.5) \times 10^{-8} \text{m}^2 \text{V}^{-1} \text{s}^{-1}$. This gives $\bar{\mu} = 0.8 \pm 0.1$. Summing Eq. S31 over six neighbouring colloids, and setting $\Phi_0^0 = 0$, we find that the only remaining term has a similar size and form to the neutral swimmer component in Fig. S2d, and is therefore negligible compared to the observed speed oscillations. Including this term in the predicted oscillations does not alter the values of b_2 and b_3 calculated from pure hydrodynamics, i.e. in Fig. S2e-f.

For a diffusiophoretic swimmer, however, the value of Φ_0^0 is determined by the reaction rate at the particle surface. From the expressions for the speed of Janus swimmers in [8], we find that, for a purely diffusiophoretic, constant mobility swimmer, $\Phi_0^0 = \pm 2au_0/\mu_p$, where the sign is positive for swimmers travelling towards their catalytic face, and negative for those which travel away, as here. We do not know the relative diffusiophoretic mobilities of the Janus particles and the static colloids, but assuming, as for the electrophoretic swimmer, $\bar{\mu} = 0.8$, we find that the finite Φ_0^0 term gives a large, pusher-type component in the speed oscillation, sufficiently large to account for approximately 50% of the observed speed variation.

FLAGELLA STAINED *E. COLI*

Construction of the smooth swimming *E. coli* strain AB1157 *cheY* has been described previously [10]. For the current work, the strain was further modified by replacement of the chromosomal copy of the *fliC* gene with a modified copy encoding a mutant FliC protein in which the serine amino acid at position 353 is replaced with a cysteine amino acid. Strain HCB1668 is a Tn5 *fliC* null derivative of AW405 in which FliC S353C is expressed from the plasmid pBAD33 [11]. This plasmid was used as a template to amplify 803 bp of *fliC* by PCR. This encompassed the AGT to TGC mutation which was flanked on each side by 400 bp of the *fliC* gene. The primers used for amplification were GCAACTCGAGCAATTGAGGGTGTCTTATACTGA and GCAAGTCGACCCTGGTTAGCTTTTGCCAACA. Restriction sites for XhoI and SalI were included. The PCR product was purified, digested with XhoI and SalI and ligated into the plasmid pTOF24, which had been digested with the same enzymes. The resultant recombinant plasmid pTOF24 *fliC* was transformed into AB1157 *cheY* and used to replace the wild type *fliC* allele with the *fliC* mutation by plasmid mediated gene

replacement using the method of [12]. Correct insertion of the mutation was verified by sequencing.

The resultant strain AB1157 *cheY* pHC60 FliC S353C was grown from a single colony in 10 ml Luria-Bertani broth containing 30 μgml^{-1} kanamycin and 5 μgml^{-1} tetracycline overnight at 30 C and 200 rpm. Bacteria were diluted 1:100 into 35 ml tryptone broth containing antibiotics as above and grown for further 4 h. Next, three washes were performed using phosphate motility buffer (6.2 mM K_2HPO_4 , 3.8 mM KH_2PO_4 , 67 mM NaCl, 0.1 mM EDTA at pH 7.0) and cells concentrated to a total volume of ~ 3 ml. To perform flagella labelling the protocol of [11] was followed. Briefly, 10 μl of Alexa Fluor 633 C5 maleimide (1 mgml^{-1} in dimethyl sulfoxide, Molecular Probes) was added to 1 ml of washed bacteria and incubated at room temperature and 100 rpm for 60 min. Three washes were performed as described above and final density was adjusted to optical density 0.3 at 600 nm in motility buffer containing 0.002 wt% TWEEN 20.

The flagella-labelled *E. coli* were observed in the sample chambers described in the main text, using confocal microscopy with 488 nm and 633 nm laser excitation on a Zeiss Confocal Microscope at 4 fps. We added 0.2 wt% TWEEN 20 to minimise adhesion of bacteria to the glass.

-
- [1] A. Edelstein, N. Amodaj, K. Hoover, R. Vale, and N. Stuurman, "Computer control of microscopes using $\mu\text{manager}$," in *Current Protocols in Molecular Biology* (John Wiley, 2010).
 - [2] S. E. Spagnolie and E. Lauga, *J. Fluid Mech.* **700**, 105 (2012).
 - [3] T.-Y. Chiang and D. Velegol, *Langmuir* **30**, 2600 (2014).
 - [4] O. S. Pak and E. Lauga, *Journal of Engineering Mathematics* **88**, 1 (2014).
 - [5] M. J. Lighthill, *Comm. Pure Appl. Maths* **5**, 109 (1952).
 - [6] K. Ishimoto and E. A. Gaffney, *Phys. Rev. E* **88**, 062702 (2013).
 - [7] E. Cummings, S. Griffiths, R. Nilson, and P. Paul, *Analytical Chemistry* **72**, 2526 (2000).
 - [8] R. Golestanian, T. B. Liverpool, and A. Ajdari, *New J. Phys.* **9**, 126 (2007).
 - [9] J. Blake and A. Chwang, *Journal of Engineering Mathematics* **8**, 23 (1974).
 - [10] I. D. Vladescu, E. J. Marsden, J. Schwarz-Linek, V. A. Martinez, J. Arlt, A. N. Morozov, D. Marenduzzo, M. E. Cates, and W. C. K. Poon, *Phys. Rev. Lett.* **113**, 268101 (2014).
 - [11] L. Turner, R. Zhang, N. C. Darnton, and H. C. Berg, *J. Bacteriology* **192**, 3259 (2010).
 - [12] C. Merlin, S. McAteer, and M. Masters, *J. Bacteriology* **184**, 4573 (2002).